Chapter 2
Constitution

2.1 General Remarks

The constitution of high interstitial steels describes the state of atomic order in thermodynamic equilibrium. It depends on the three variables of state: concentration of alloying elements in iron, temperature and pressure. A region that is in the same state of order is known as a phase. Nitrogen is a volatile element and therefore the gas phase and especially the partial pressure of N_2 has to be taken into account. The liquid phase appears during melting, solidification and welding. Of the solid state phases austenite, δ-ferrite, carbides, nitrides and sigma phase are to be expected. To cope with such a complex alloy system the commercial software program THERMO-CALC^{TM}, version R with TCFE4 database [1] was used to calculate the constitution of multi-component HIS.

It depends on experimental data and theoretical models covering a wide range of steel compositions by minimizing the Gibb's free energy [2]. The program provides phase diagrams as isothermal or isoplethal sections through a system. Also the mole, mass or volume fraction of phases in a given steel may be plotted over the temperature. In addition the chemical composition of each phase is available. In the high temperature range from solidification to solution annealing, which are of practical importance, less deviation from the calculated equilibrium is to be expected than at lower temperatures. However during quenching the kinetics of precipitation are of interest only. It is shown in the next chapter that the atoms in homogeneous austenite are not necessarily distributed evenly, but that microsegregation (mm range) or short range atomic decomposition (clustering, nm range) may cause a chemical inhomogeneity which is not covered by the calculations. Tramp elements are not considered to reduce the computing time except for manufactured grades.

Limited experimental verification was in good agreement with the simulation. Therefore the calculated phase diagrams are taken as a reasonable guideline to reveal tendencies.

H. Berns et al., *High Interstitial Stainless Austenitic Steels*,
Engineering Materials, DOI: 10.1007/978-3-642-33701-7_2,

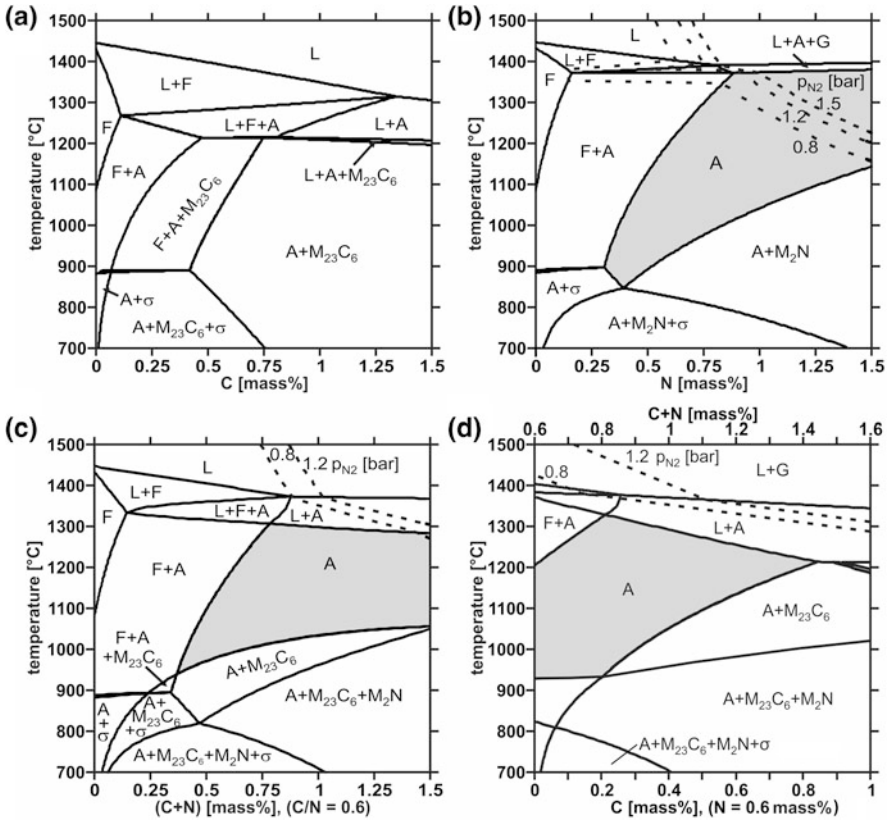

Fig. 2.1 Isoplethal phase diagram of Fe-18Cr-18Mn in dependence of (**a**) Carbon content. **b** Nitrogen content. **c** C + N content at constant C/N = 0.6. **d** C content at constant N = 0.6 mass %, i.e. increasing C/N. Shaded area = homogeneous austenite

2.2 Variation of Interstitial Content

To start with, the alloy system Fe-18Cr-18Mn is studied in respect to additions of C, N or C + N, because the commercial grade Cr18Mn18N0.55 has been successfully manufactured and applied. In fact, nitrogen opens up a wide field of homogeneous austenite (shaded area in Fig. 2.1b) while carbon provides austenite only in combination with carbide $M_{23}C_6$ and/or ferrite (Fig. 2.1a). This is to say that a steel alloyed with 18 mass % Cr to make it stainless and with the same content of Mn to stabilize austenite cannot be strengthened by interstitial carbon without precipitation of carbides which consume chromium and impair toughness.

In contrast the high solubility of nitrogen in austenite during solution annealing (Fig. 2.1b) offers intensive strengthening within the target range of 0.8–1.1 mass % N without detrimental precipitation of M_2N nitrides. However, the N_2 isobars reveal that a partial pressure $p_{N2} = 0.8$ bar nitrogen in air is not sufficient

to dissolve 0.8–1.1 mass % N in the melt. At lower contents solidification passes through a regime of ferrite whose solubility for nitrogen is much lower than that of austenite. The resulting degassing may cause boiling or foaming of the solidifying melt or pores in the solid material. Pressure metallurgy is a means of raising the nitrogen content in the melt to a level which assures a fully austenitic solidification. It is important to note that p_{N2} governs the uptake of nitrogen to the equilibrium content, but that the formation of bubbles at the beginning of degassing depends on the total pressure including the ferrostatic part of the melt which somewhat eases the problem in respect to the calculations.

The concept of alloying with C + N is now applied to the basic composition of steel Cr18Mn18N0.55 to avoid pressure metallurgy (Fig. 2.1c). The C + N content is plotted along the abscissa at a selected C/N ratio in mass %. The atomic ratio is smaller by [1−(12/14)] 100 ≈ 14 %. The shaded phase field of homogeneous austenite is sufficiently large to dissolve 0.8–1.1 mass % C + N at a solution anneal temperature T_{SA} of e.g. 1100 °C. As in Fig. 2.1b the L-F-A triple point remains just below 0.9 mass % of interstitials but the corresponding p_{N2} is lowered from 1.5 to 0.8 bar and a fully austenitic solidification is to be expected (Fig. 2.1c). This means that the partial replacement of N by C is as effective in fending off δ-ferrite but comes with less volatility of the remaining nitrogen. The solidus temperature T_S is lowered by carbon, but the temperature of beginning precipitation T_P is hardly changed within the interstitial range of interest. The type of precipitate turns from M_2N to $M_{23}C_6$ though, which is followed by M_2N at lower temperatures.

The addition of carbon to commercial steel Cr18Mn18N0.55 will reduce the content of δ-ferrite during solidification and allow of more nitrogen in the melt. Therefore Fig. 2.1d starts from 0.6 mass % N and directly demonstrates the effect of carbon implying an increase of the C/N ratio. The L-F-A triple point is located at about 0.25 mass % C and the corresponding temperatures T_S and T_P are about 1320 and 950 °C respectively.

At higher carbon contents the range of homogeneous austenite between T_S and T_P is narrowed and with it the interval for hot working and solution annealing. At the example of the commercial grade Fig. 2.1c and d clearly demonstrate that the C/N concept is suited to increase the interstitial content by melting at normal pressure of air, but that there is a limit to the optimal carbon content.

2.3 Effect of C/N Ratio

An isothermal section through the Fe-18Cr-18Mn-C–N system at $T_{SA} = 1100$ °C outlines the shaded target area of homogeneous austenite (Fig. 2.2). It is encased by ferrite to the left, M_2N to the right and $M_{23}C_6$ above. The carbon content of austenite grows from (mass %) 0.3 at 0.2 N to almost 0.8 at 1.1 N. This underlines the beneficial effect of jointly alloying C + N in respect to the intended increase of the interstitial content in austenite. It may be raised further by a higher T_{SA},

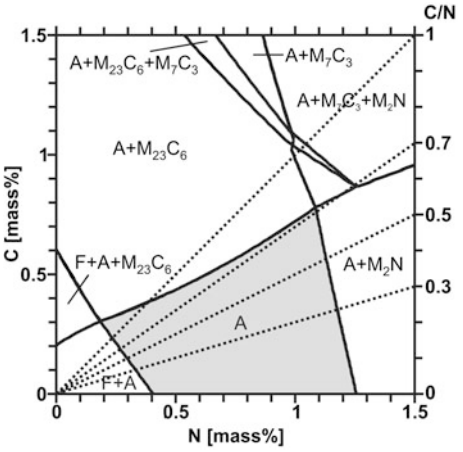

Fig. 2.2 Isothermal phase diagram at 1100 °C of Fe-18Cr-18Mn-C–N. The dotted lines represent different C/N ratios. Shaded area = homogeneous austenite

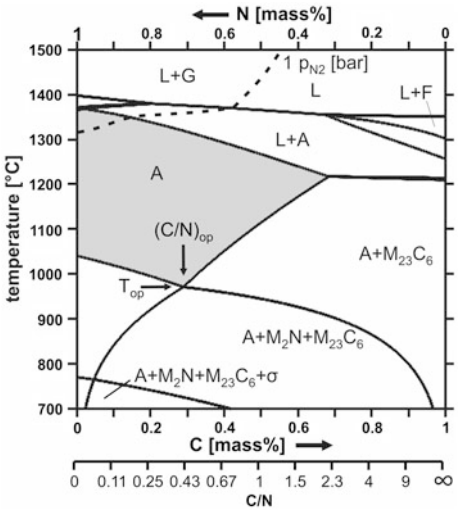

Fig. 2.3 Isoplethal phase diagram of Fe-18Cr-18Mn in dependence of the C/N ratio at C + N = 1 mass %. At $(C/N)_{op}$ the shaded phase field of homogeneous austenite extends to the lowest temperature T_{op}

because the phase field of austenite is expanded at the expense of precipitates, but gives way to ferrite on the left.

The dotted lines in Fig. 2.2 represent C/N ratios. At C/N = 1 the respective line cuts the austenitic phase field at the low interstitial end, while at 0.7 it touches the point of highest interstitial solubility. At 0.5 it runs in parallel to the A/A + $M_{23}C_6$ boarder. The results of this isothermal plot suggest C/N < 0.7. In an isoplethal section through the Fe-18Cr-18Mn system the C/N ratio is varied by plotting C and N in opposite directions along the abscissa at a constant content of C + N = 1 mass % (Fig. 2.3). It is evident that the phase field of homogenous austenite extends to the lowest temperature T_{op} at $(C/N)_{op}$ = 0.41 at which M_2N and $M_{23}C_6$ start to precipitate simultaneously. The index "op" refers to optimal conditions in respect to

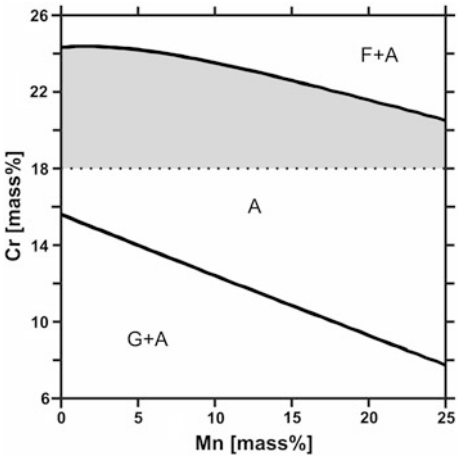

Fig. 2.4 Isothermal phase diagram at 1100 °C of Fe–Cr-Mn-0.3C-0.6 N. Shaded area = phase field of homogeneous austenite with ≥18 mass % Cr, C + N = 0.9, C/N = 0.5

retarding the begin of precipitation during quenching from T_{SA}. To the left of $(C/N)_{op}$ M_2N starts to precipitate at $T_P > T_{op}$ and to right this holds true for $M_{23}C_6$. In the middle part of the C/N range a fully austenitic solidification prevails.

2.4 Variation of Substitutional Content

The basic substitutional elements are chromium and manganese. Molybdenum and copper are of interest in respect to corrosion resistance. Tramp elements can affect the constitution.

2.4.1 Chromium and Manganese

The influence of these elements on the constitution is demonstrated by an isothermal section at $T_{SA} = 1100$ °C and a C + N content within the target range (Fig. 2.4). The plot suggests a wide phase field of homogeneous austenite of which more than half does not apply, if a minimum content of 18 mass % Cr is chosen to promote corrosion resistance. The lower the manganese content the closer the alloys come to superheated stainless tool steel with retained austenite and little ductility. In addition a partially ferritic solidification and a loss of nitrogen is to be expected. The higher the manganese (and chromium) content, the lower the concentration of free electrons [3]. Therefore the Mn content in Fig. 2.5a is varied only moderately in the range of 18 ± 5 mass %. Unexpectedly ferrite is stabilised by Mn at 1100 °C and $M_{23}C_6$ as well. However, the austenitic phase field grows at the expense of M_2N. It shrinks in respect to $M_{23}C_6$ by a higher C/N ratio (Fig. 2.5b) and by a lower temperature (Fig. 2.5c) which may entail a shift of the

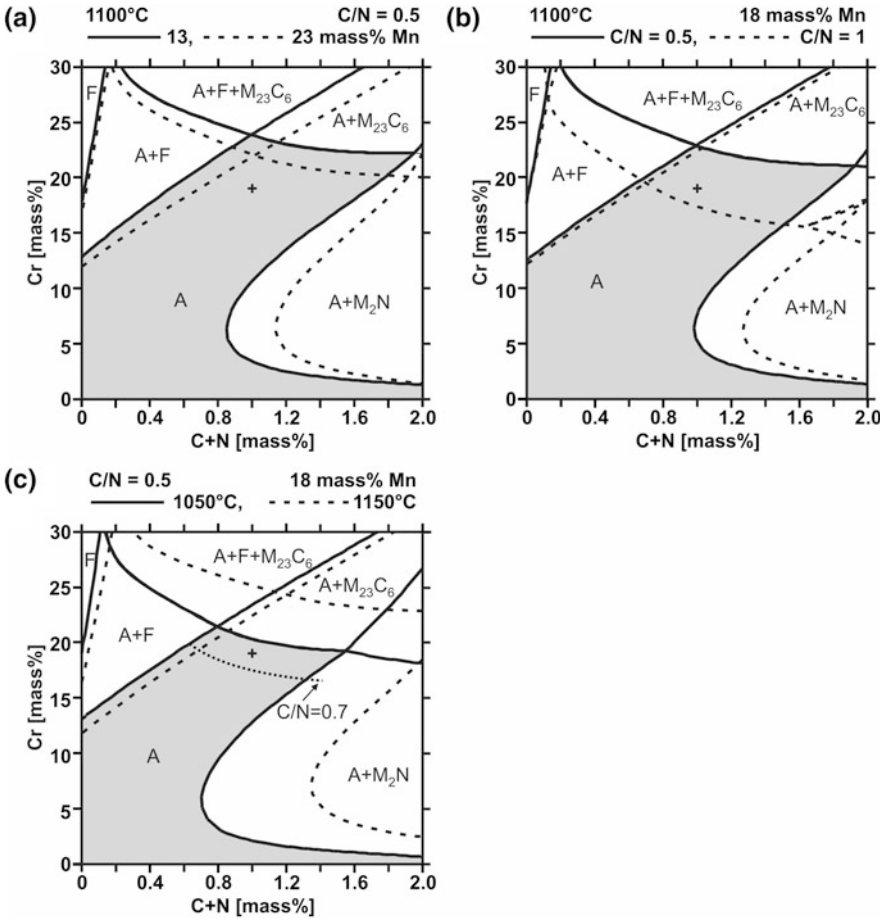

Fig. 2.5 Isothermal phase diagrams showing the effect of Cr and C + N content and of (**a**) Mn content. **b** C/N ratio. **c** Temperature. Shaded phase field = homogeneous austenite, dotted line = C/N = 0.7 at 1050 °C, (+) = target composition

target point (+) at (mass %) 18 Cr and 1 (C + N) from the A to the A + $M_{23}C_6$ phase field. As expected, Cr stabilises ferrite and C + N are required to obtain austenite which loses ground to $M_{23}C_6$ and the more so the higher C/N (Fig. 2.5b).

After this view on the constitution at solution anneal temperature T_{SA} in Figs. 2.4 and 2.5 the situation at higher and lower temperatures is of interest. At the example of two steels it is demonstrated that an increase from 13 to 23 mass % Mn lowers the temperature range of solidification but prevents ferrite and raises the temperature of beginning N_2 gas evolution (Fig. 2.6). At temperatures below T_{SA} manganese enhances the precipitation of $M_{23}C_6$ at the expense of M_2N as already visible in Fig. 2.5a. The promotion of σ-phase by Mn is confined to such a low range of temperature that it is likely to be subdued during quenching. The

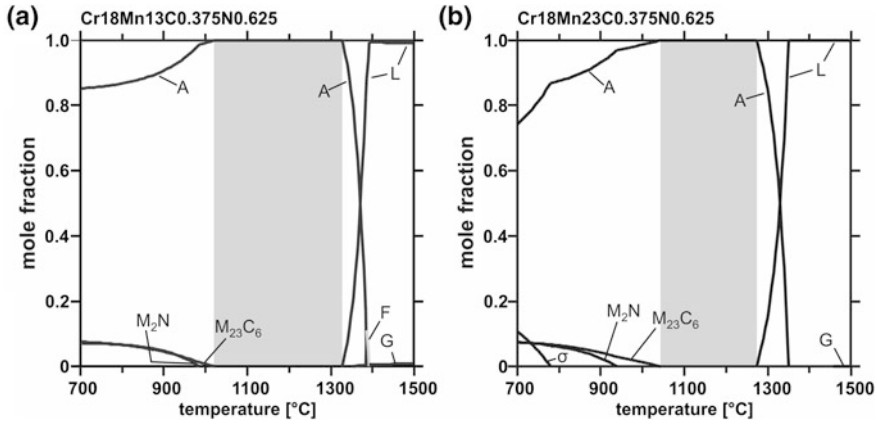

Fig. 2.6 Phase fraction of two steels with (mass %) 18Cr and 1 (C + N) at C/N = 0.6 but different Mn content in dependence of temperature, shaded area = homogeneous austenite

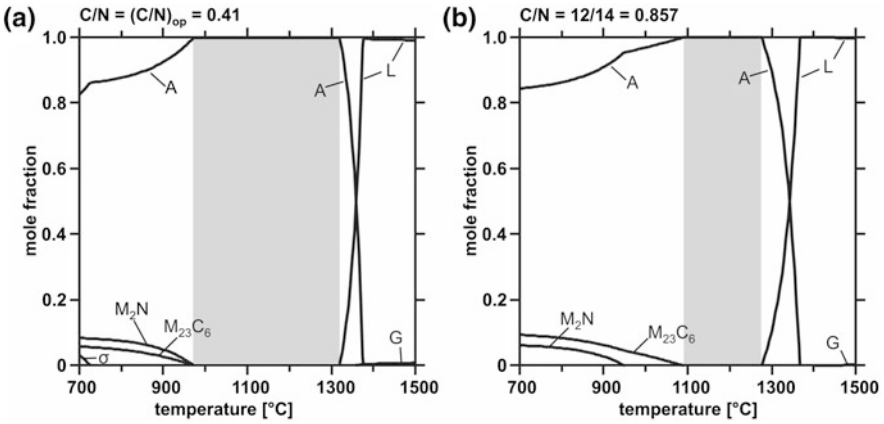

Fig. 2.7 Phase fraction of steel Cr18Mn18(C + N)1 at two different C/N ratios in dependence of temperature, shaded area = homogeneous austenite

jump from 13 to 23 mass % Mn narrows the regime of homogeneous austenite on either side (Fig. 2.6). Thus 18 mass % Mn seem to be a good compromise between high T_S, low T_P and suppression of ferrite as well as gas. The respective steel Cr18Mn18(C + N)1 is now analysed as to the influence of the C/N ratio (Fig. 2.7). To stay below $(C/N)_{op}$ (Fig. 2.3) would mean to give away interstitial solubility and strength. A mole fraction of 1 would correspond to C/N = 0.857 which according to Fig. 2.3 would require $T_{SA} > 1100$ °C. As for the higher Mn content in Fig. 2.6, the higher C/N ratio narrows the range of homogeneous austenite on both sides (Fig. 2.7). The results suggest not to exceed these limits of the C/N range.

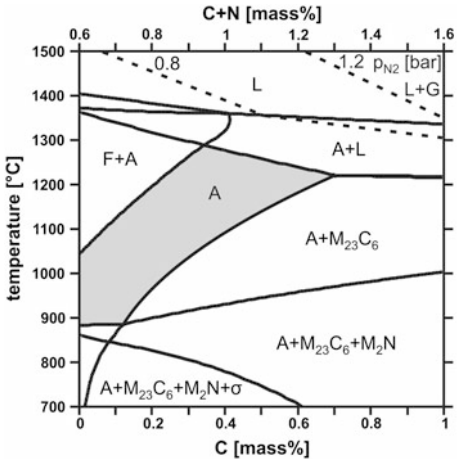

Fig. 2.8 Isoplethal phase diagram of Fe-20Cr-18Mn-0.6N–C, shaded area = homogeneous austenite

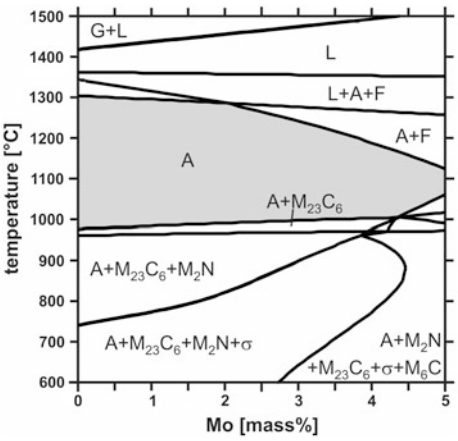

Fig. 2.9 Isoplethal phase diagram of Fe-18Cr-18Mn-0.6N-0.25C-Mo

In Fig. 2.4 chromium contents below 18 mass % were already excluded because of corrosion resistance. Contents above this level are likely to improve this property but promote ferrite and $M_{23}C_6$. This becomes immediately evident if Fig. 2.8 is compared with Fig. 2.1d. The shaded phase field of austenite with 20 mass % Cr is reduced but still allows steels in the upper interstitial target range.

2.4.2 Molybdenum and Copper

Alloying stainless steels with molybdenum is a common measure to impede pitting corrosion [4]. As this element is a carbide former and a ferrite stabilizer, the question is what content is permitted in austenitic CrMnCN steels. The influence

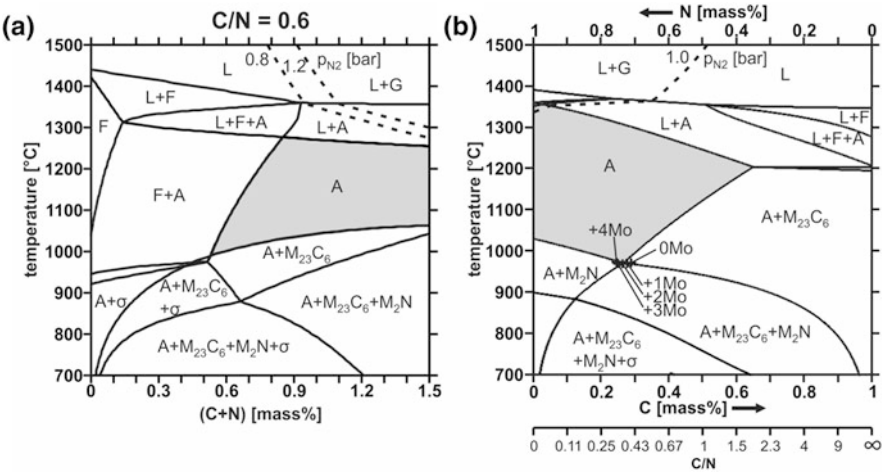

Fig. 2.10 Isoplethal phase diagrams of Fe-18Cr-18Mn-2Mo in dependence of **a** C + N content at C/N = 0.6. **b** C/N ratio at C + N = 1, the pairs of $(C/N)_{op}$ and T_{op} are marked by (+) for different Mo contents

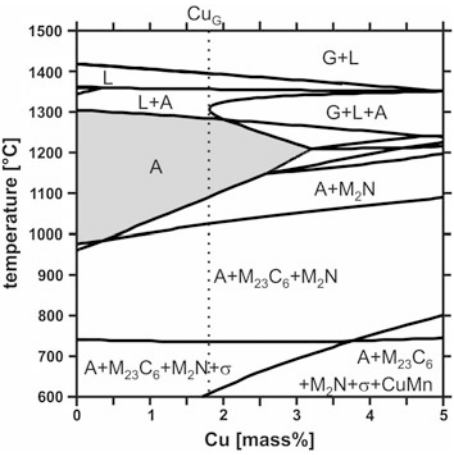

Fig. 2.11 Isoplethal phase diagram of Fe-18Cr-18Mn-0.6N-0.25C-Cu

of Mo on the constitution is depicted in Fig. 2.9 at the example of steel Cr18Mn18N0.6C0.25. The gas phase is shifted to higher temperatures as Mo lowers the activity of nitrogen in the melt. Ferrite is stabilised to lower temperatures but—up to ≈ 2 mass % Mo—not below ≈1300 °C which allows hot working in the range of homogeneous austenite. The temperature T_P of beginning precipitation ($M_{23}C_6$ followed by M_2N) is hardly raised and at 2 mass % Mo stays just below 1000 °C. The temperature of σ precipitation is raised, though. The addition of ≤2 mass % Mo to the above steel appears to be feasible.

Starting from the previous example, the influence of C + N and C/N is investigated next (Fig. 2.10). Compared to Fig. 2.1c the austenitic phase field in

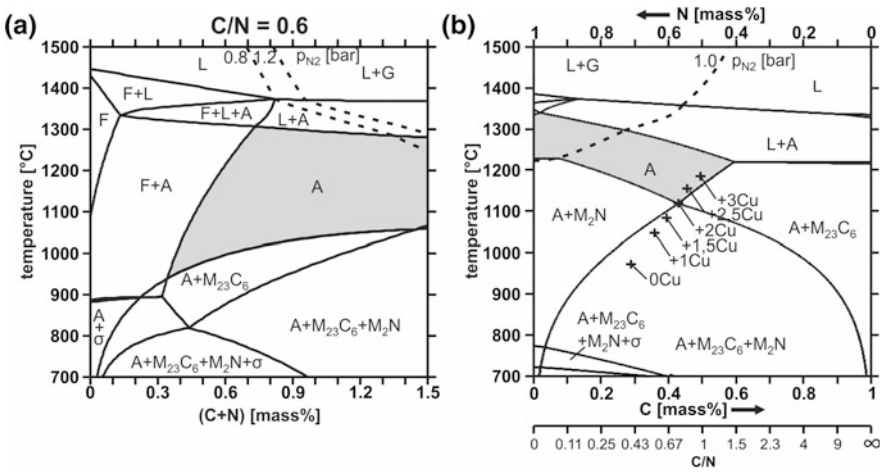

Fig. 2.12 Isoplethal phase diagram of Fe-18Cr-18Mn-2Cu in dependence of **a** C + N content at C/N = 0.6. **b** C/N ratio at C + N = 1, the pairs of $(C/N)_{op}$ and T_{op} are marked by (+) for different Cu contents

Fig. 2.10a is reduced by ferrite to the left and liquid above. In respect to Fig. 2.3 T_{op} and $(C/N)_{op}$ in Fig. 2.10b are changed only moderately by up to 4 mass % Mo.

Stainless steels are alloyed with copper to reduce general corrosion e.g. in non-oxidising acid solution [4]. In contrast to molybdenum, copper stabilises austenite and raises the activity of interstitials. This is reflected in Fig. 2.11 indicating a steep rise of T_P. At $Cu_G \approx 1.8$ mass % the evolution of N_2 gas ends the range of homogeneous austenite. At this Cu level the range of 0.8–1.1 mass % C + N leads to an austenitic solidification and a reasonable T_{SA} (Fig. 2.12a). The pairs of $(C/N)_{op}$ and T_{op} at 1 mass % C + N increase considerably with the Cu content (Fig. 2.12b). While the addition of 2 mass % Mo or Cu seem to be feasible, joint alloying of both elements to this level leads to a dramatic shrinkage of the austenitic phase field which would make it difficult to process such a steel.

2.4.3 Tramp Elements

Small quantities of the strong carbide and nitride formers vanadium, niobium and titanium may result in MX precipitates. In view of the high interstitial content of HIS these precipitates hardly dissolve at T_{SA} and would represent an additional phase.

Silicon raises the activity of C and N and thereby promotes precipitation. This is reflected for Fe-18Cr-18Mn-1(C + N) by a shift of the pairs $(C/N)_{op}$ and T_{op} from 0.408 and 971 °C at zero Si to 0.486 and 1026 °C at 0.5 mass % Si and further to

0.560 and 1075 °C at 1 mass % Si. To avoid a detrimental increase of T_{op} by up to 100 °C it is recommend to not fully exploit the range of Si $\leq$ 1 % given e.g. in EN10088 for austenitic steels, but to keep its content as low as possible.

2.5 Selection of Steels

The phase field of homogeneous austenite is the target area of HIS to be reached by solution annealing and preserved by quenching. An austenitic solidification is desirable to transfer nitrogen from the melt to the austenite without degassing. To keep the concentration of free electrons high and with it the ductile metallic character of interatomic bonding a reduction of substitutional alloy content, namely of Cr, Mn, Mo, would be helpful (see Sect. 3.1.3). However, the experience with HIS Mn17Cr15N0.43C0.39 and general knowledge on stainless steel speak for 18 mass % Cr. As shown above, 18 mass % Mn are a reasonable match to avoid ferrite during solidification.

The interstitial content is aimed at $\geq$0.8 mass % C + N to boost strength. In view of experience with HNS and the calculations above the envisaged upper limit of 1.1 mass % C + N is confirmed to avoid problems during hot working and heat treatment. As to the C/N ratio, one has to start from the soluble content of nitrogen in alloys with 18 mass % of Cr and Mn each at normal pressure of air. It slightly depends on the carbon content, but 0.6 mass % N seems to be a fair value to start with. Combining the C + N content and the C/N ratio in mass % we arrive at $C + N = N\ [(C/N) + 1]$. Inserting $N = 0.6$ and $(C/N)_{op} = 0.41$ the C + N content is 0.85. Higher interstitial contents have to rely on more carbon which entails $C/N > (C/N)_{op}$ and $T_P > T_{op}$.

Based on these constitutional considerations three steels with 18 mass % of Cr and Mn each were selected: one at the lower end of the C + N target range, one at the upper end and one in the middle. These three new HIS were molten and hot worked on an industrial scale and designated according to their C + N content, times 100, i.e. CN85, CN96 and CN107 (Table 2.1).

To these Mo and Cu were added by remelting a smaller batch. A series of HIS with 0.65–1.15 mass % C + N was produced as castings. In accordance with European standards the designation is preceeded by "G". A few reference steels are listed of which CrNi represents a standard low interstitial grade, MnC a high carbon Hadfield steel and CrMnN a high nitrogen steel. The grades MnCr82 and MnCr70 are reference HIS of lower chromium and interstitial content. For the investigation of structure (Chap. 3) and properties (Chap. 4) premachined specimens were solution annealed, quenched and machined to final size. Details of HIS manufacture are given in Chap. 5.

Table 2.1 Chemical composition in mass % of the austenitic steels investigated

No.	designation	C	N	P	S	Cr	Mn	Si	Mo	Cu	Ni	C + N	C/N
1	CN85	0.26	0.59	0.018	0.001	18.3	18.5	0.26	0.04	–	0.26	0.85	0.44
2	CN96	0.344	0.614	0.021	0.002	18.2	18.9	0.30	0.06	–[(a)]	0.34	0.96	0.56
3	CN107	0.489	0.578	0.026	<0.001	18.8	18.9	0.43	0.07	–[(a)]	0.40	1.07	0.85
4	CN94Mo1	0.324	0.620	0.025	<0.001	17.9	19.0	0.23	0.96	–	0.32	0.94	0.52
5	CN103Mo1	0.452	0.582	0.027	<0.001	18.3	18.6	0.42	0.94	–	0.38	1.03	0.78
6	CN96Cu2	0.370	0.594	0.023	<0.001	17.6	19.3	0.18	0.04	1.90	0.28	0.96	0.62
7	GCN65	0.033	0.616	0.017	0.002	19.9	18.0	0.33	0.04	0.398	0.47	0.65	0.05
8	GCN88	0.228	0.654	0.017	0.001	20.2	18.0	0.28	0.04	0.316	0.39	0.88	0.35
9	GCN98	0.400	0.583	0.018	< 0.001	20.1	18.1	0.14	0.04	0.306	0.40	0.98	0.69
10	GCN115	0.512	0.641	0.018	<0.001	19.9	18.0	0.33	0.06	0.268	0.46	1.15	0.80
11	GCN85	0.256	0.596	0.017	<0.001	18.3	18.4	0.54	0.02	–[(a)]	0.10	0.85	0.43
12	CrNi	0.004	0.050	0.020	0.022	18.7	1.9	0.57	–	–	9.04	0.05	0.08
13	MnC	1.190	0.009	0.090	0.014	0.2	12.1	0.49	–	–	0.1	1.20	132
14	CrMnN	0.040	0.880	–	–	21.0	23.1	0.30	0.2	–	1.5	0.92	0.05
15	MnCr82	0.387	0.431	0.044	0.007	14.7	17.2	0.48	<0.02	–	<0.07	0.82	0.90
16	MnCr77	0.319	0.447	–	–	12.0	25.4	–	–	–	–	0.77	0.71

No. 1–6 = Hot worked steel, 7–10 = Centrifugal castings, 11 = Sand casting, a section of which was hot worked → CN85×, 12–16 = Hot worked reference steels

[(a)] $V < 0.07$

References

1. Software System and Users Guide (2008) Thermo-Calc Software AB SE- 11347 Stockholm
2. Saunders N (1995) Phase diagram calculation for high-temperature structural materials. Phil Trans Royal Soc London A351:543–561
3. Shanina BD, Gavriljuk VG, Konchitz AA, Kolesnik SP (1998) The influence of substitutional atoms upon the electron structure of the iron-based transition metal alloys. J Phys Condensed Matter 10:1825–1838
4. Heimann W, Oppenheim R, Wessling W (1993) Stainless steels. In: Steel, vol 2. Springer, Berlin, pp 382–422

http://www.springer.com/978-3-642-33700-0

High Interstitial Stainless Austenitic Steels

Berns, H.; Gavriljuk, V.; Riedner, S.

2013, X, 170 p., Hardcover
ISBN: 978-3-642-33700-0